Available online at www.sciencedirect.com
SCIENCE DIRECT®
Journal of Catalysis 225 (2004) 69–77
JOURNAL OF CATALYSIS
www.elsevier.com/locate/jcat

Formation of hydrogen peroxide from H_2 and O_2 over a neutral gold trimer: a DFT study

David H. Wells Jr., W. Nicholas Delgass, and Kendall T. Thomson *

School of Chemical Engineering, Purdue University, West Lafayette, IN 47907, USA

Received 6 January 2004; revised 15 March 2004; accepted 18 March 2004

Available online 24 April 2004

Abstract

Our density-functional theory study of the formation of hydrogen peroxide over a neutral Au_3 cluster details a reaction path with activation barriers less than 10 kcal/mol. The reactions proceed on the edges and one side of the triangular Au_3 cluster which makes this mechanism viable for a cluster in contact with a support surface. The Au_3 cluster remains in a triangular geometry throughout the reaction but the electron population on the Au trimer during the catalytic cycle proper, as calculated with the Natural Bond Orbital method, varies from a charge of $+0.304$ (cationic) ($Au_3O_2H_2$) to -0.138 (anionic) (Au_3H_2). Au_3 in the reaction initiation intermediate, Au_3O_2, is also cationic in character with a charge of $+0.390$. It is interesting to note that the interaction of Au_3 with a model oxidic support, TS-1, was essentially neutral in character, the Au_3 charge population being -0.044. Formation of hydrogen peroxide does not involve breaking the O–O bond, but does break the H–H bond in a step that is rate limiting under standard conditions. The highest energy barrier in the cycle is 8.6 kcal/mol for desorption of H_2O_2 from Au_3H_2. Adsorption of H_2O_2 on this site is unactivated. This route to formation of hydrogen peroxide combined with existing mechanisms for epoxidation by H_2O_2 over TS-1 gives a fully plausible, energetically favorable, closed cycle for epoxidation of propylene by H_2 and O_2 over Au/TS-1 catalysts. Thus, isolated molecular gold clusters can act as viable sites for this reaction.

Keywords: Epoxidation; Hydrogen peroxide; Au; Gold; Au cluster catalysis; DFT; Density functional theory

1. Introduction

Research on the epoxidation of propylene by H_2 and O_2 over Au supported on titanium-containing oxidic supports has led to many interesting results but no complete explanation of the reaction mechanism involved [1–19]. One of these catalysts, Au/TS-1, has a relatively well-defined crystalline support (titanium silicalite [20]), but despite the crystalline nature of the support, this catalyst system is still complicated enough to hamper definitive experimental investigation. Experimental claims have been made that Au nanoparticles with approximately 2 nm diameter supported on pure titania give the highest selectivity to propylene oxide, while smaller Au particles give propane as a major product, and larger bulk-like Au particles are simply not reactive [21]. In related Au-containing catalytic systems, experimental evidence has been found that nonmetallic gold is active: water gas shift [22] and CO oxidation [23,24]. Several proposals have been put forth as to the nature and role of active gold sites. One proposal based on theoretical study is that the unusual activity of small supported particles of Au, "may in part be due to high step densities on the small particles and/or strain effects due to the mismatch at the Au–support interface" [25]. High level computational analysis of the reaction is inhibited by the complexity and scale of the system. Electronic structure calculations looking for unique qualities of a 2 nm Au cluster with hundreds of gold atoms on a TS-1 crystal surface of comparable size would be impossible with existing computers using current density-functional theory (DFT) tools. Smaller gold ensembles provide a more accessible alternative, and, as well, may be of a size that is highly active, though the presence of such small clusters in working catalysts is still an open question. Small Au clusters of a few atoms would not be excluded from entering a TS-1 crystallite due to size limitations of the pore system (~ 5.5 Å). This affords close proximity of small Au clusters with a larger number of Ti sites than just those on the outside of a TS-1

* Corresponding author.
E-mail addresses: wellsd@purdue.edu (D.H. Wells), delgass@ecn.purdue.edu (W.N. Delgass), thomsonk@ecn.purdue.edu (K.T. Thomson).

0021-9517/$ – see front matter
doi:10.1016/j.jcat.2004.03.028

crystallite (in a 150-nm TS-1 crystallite there are approximately 50 times as many internal Ti sites as on the external surface of the crystallite).

Small atomic-sized Au clusters are in the range where gas-phase adsorption of H_2 and O_2 on cluster cations has been shown experimentally (<15 atoms) [26]. Therefore, interaction with H_2 and O_2 is likely to be important in this system. Small Au clusters inside TS-1 in proximity to active Ti substitution sites may function by catalyzing the formation of hydrogen peroxide, which does selective oxidation of propylene at the Ti site. Experimentally, it has already been established that Au particles supported on alumina are capable of generating hydrogen peroxide from H_2 and O_2 in solution at low temperatures [27]. Recent work has also identified OOH species with inelastic neutron scattering when H_2 and O_2 are reacted over Au/TiO_2 catalyst [28]. If the role of Au in the Au/TS-1 catalyst is to generate H_2O_2 from H_2 and O_2, the remaining steps of the epoxidation mechanism may be described by any one of several mechanistic proposals for this reaction in the literature [8,29–34]. Previously we have proposed that heterogeneous epoxidation of propylene by H_2O_2 occurs over Ti sites in TS-1 zeolites with adjacent Si lattice vacancies [35]. Such vacancies are relatively abundant in even "well-made" TS-1 [36] and lead to the frequent occurrence of Ti/defect pairs [30]. That mechanism combined with H_2O_2 production from H_2 and O_2 over small Au clusters may fully explain the catalytic nature of Au/TS-1 epoxidation catalysts.

In what follows we provide the details for formation of H_2O_2 over the neutral Au_3 cluster from H_2 and O_2 based on DFT calculations. We first establish the geometry of a Au_3 cluster with adsorbed oxygen. This is important since it differs from the geometry of the bare gas-phase cluster. The preferred triangular Au_3 cluster geometry is the starting point for subsequent geometry optimizations. The entrance channel is O_2 addition to a bare Au_3 cluster followed by H_2 addition. Both of these steps are unactivated or have very low (<1 kcal/mol) barriers. The catalytic cycle itself has two transition states and four intermediate stable configurations (O_2 addition during the cycle is unactivated). Geometries along the entrance channel path and for the unactivated O_2 addition step are shown and discussed.

2. Computational method

All calculations were conducted using the Gaussian98 [37] suite of programs. We used density-functional theory with the 1988 exchange functional [38] of Becke and Purdue–Wang's 1991 correlation energy functional (BPW91) [39–42]. The Los Alamos LANL2DZ [43,44] effective core pseudo-potentials (ECP) and valence double zeta basis set for gold was utilized as well as the D95 [45] valence double zeta basis sets for hydrogen and oxygen. The choice of functional was dictated in part by other research being conducted in conjunction with this work which involves small Au clusters. Since the metallic clusters can be poorly represented by B3LYP [37] we have chosen BPW91 as a reasonably equivalent alternative. The accuracy of the BPW91 functional in predicting atomization energies for a set of species including third row atoms is about ± 5 kcal/mol [46]. The accuracy of energy differences we calculate for Au_3 species with adsorbates is likely to be lower due to cancellation of systematic errors over such a narrow molecular range. Basis set superposition errors were not calculated as they would be a small factor of several kcal/mol and a relatively constant energetic offset across the cluster models we compared. Previously we have computed adsorption behavior of O_2 on small Au clusters [47] and found agreement with experimental results [26] illustrating that density functional theory using the LANL2DZ pseudopotentials is an adequate descriptor of Au cluster chemistry. All transition states were identified by the synchronous transit-guided quasi-Newton (STQN) method of Peng and Schlegel [48]. This technique uses geometries for the reactants and products as its starting points and searches via linear or quadratic transit for a geometry close to the transition state. Natural bond orbital (NBO) analysis of the electron population on each atomic center was performed with the program available within the Gaussian98 and Gaussian03 suites [49].

3. Results and discussion

3.1. Au_3 cluster geometry

The catalytic cycle investigated here is over a generally triangular conformation of neutral Au_3. Two earlier computational studies of Au_3 found a triangular geometry with asymmetry due to Jahn–Teller distortion in the ground state [50,51]. Grönbeck and Andreoni [51], using periodic density-functional theory, calculated the energy difference between two similar triangular geometries and a linear configuration. The BLYP functional predicted the linear geometry to be 2.8 kcal/mol higher in energy. Bravo-Perez and co-workers also found the linear geometry to be higher in energy by 5–6 kcal/mol using MP2 and MP4 ab initio methods. Using the BPW91 density functional, we have found the ground state to be the linear geometry with an energy difference of about 1 kcal/mol to the lowest energy triangular geometry. A more recent calculation [52] based on periodic density-functional theory also finds the linear geometry to be the lowest energy state for the bare Au_3 cluster. With adsorption of O_2 on the linear cluster, the preferred geometry changes to triangular. O_2 adsorption induces charge separation in the Au_3 chain leading to energy minimization in a folded conformation. Mulliken electron population differences on the atoms in the gas-phase linear molecule are less than 0.01 electrons per Au atom, while in the triangular geometry, differences are 0.04 or larger. Since at room temperature and above, both conformations would be popu-

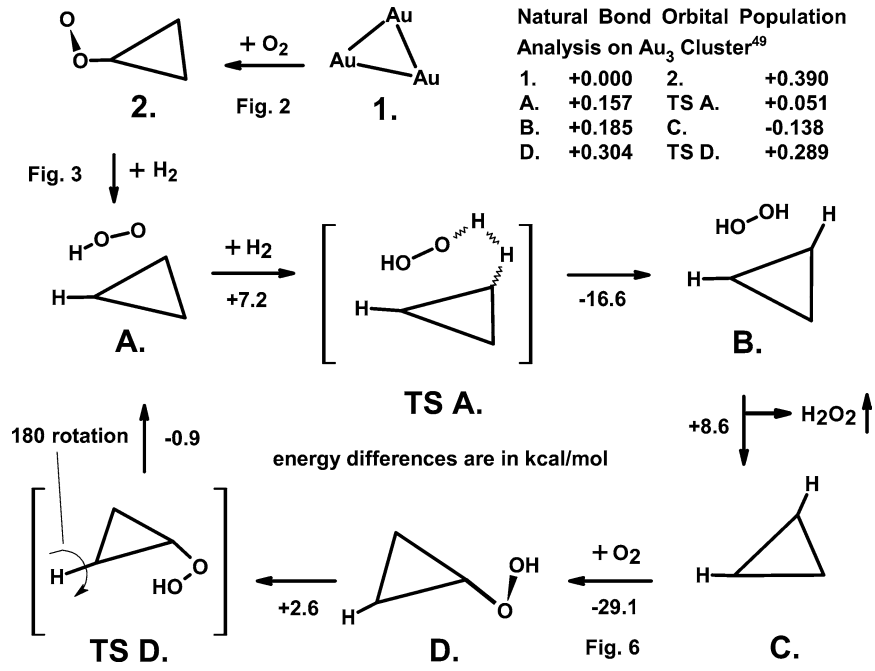

Fig. 1. Catalytic cycle for formation of H_2O_2 over Au trimer with two transition state geometries identified with square brackets. The main cycle proceeds from structure **A** in clockwise fashion. The uncoordinated Au atom of the cluster in **TS D** is different from the uncoordinated Au atom in structure **A**, but 180° rotation about the plane of the Au cluster will show that these are equivalent. Energy differences are shown in kcal/mol under each reaction arrow.

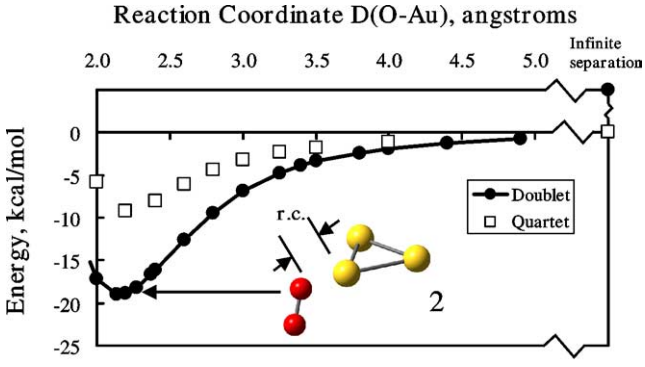

Fig. 2. The energy profile (at 0 K without zero-point energy corrections) for oxygen addition in the entrance channel forming intermediate **2** along the indicated reaction coordinate (r.c.), the smallest O–Au distance. The spin transition for the system from quartet spin to doublet spin can occur in the reaction coordinate region from 4 to 5 Å without any activation barrier.

lated, we have assumed the triangular geometry as a starting point throughout these calculations, though absolutely no constraints were made to the cluster geometry while searching for transition states and following reaction pathways.

3.2. Entrance channel reactions

The entry channel to the catalytic cycle is a two step process illustrated in Fig. 1 going from intermediate **1** to intermediate **A**. The first step is addition of O_2 to the bare cluster. Nondissociative O_2 adsorption in bent end-on fashion to small atomic-sized Au clusters has been reported previously [47,52,53]. In our work with the larger Au_{10}^- cluster [47], molecular oxygen adsorbed in both side-on (19 kcal/mol binding energy) and end-on (3–6 kcal/mol binding energy) configurations. The end-on arrangement has a weaker binding energy by 13–16 kcal/mol depending on the particular end-on binding location. Side-on binding of a single O_2 molecule to a neutral triangular Au_3 cluster was reported by Mills and co-workers to be the lowest energy configuration based on their computations [54]. Their calculated O_2 binding energy was 21 kcal/mol, very similar to our result of 22 kcal/mol. We found the binding energy for O_2 in the end-on geometry to be slightly less, 19 kcal/mol. We reason that since side-on bonded O_2 is slightly more tightly held, it may be less likely to react with H_2, so our investigation has begun with the end-on geometry (intermediate **2** in Fig. 1). The energy barrier for conversion of side-on bonded O_2 to end-on bonded is 6 kcal/mol, smaller than other limiting steps in the cycle (vide infra). Thus both forms of adsorbed oxygen on the Au trimer are reactive. Addition of triplet spin O_2 to the bare Au_3 cluster, which has doublet spin configuration in the ground state, requires a spin transition to reach the stable doublet spin state of Au_3O_2. This spin transition occurs early along the reaction path as shown in Fig. 2, which also gives the energy along the path for O_2 adsorption in both spin systems. At infinite separation of O_2 and Au_3, the energy difference between doublet and quartet (triplet O_2 + doublet Au_3) spin for the combined system is calculated to be 38.5 kcal/mol. This is the difference between (sigma) singlet ($^1\Sigma_g$) and triplet di-oxygen which experimentally is 37.5 kcal/mol [55]. The same results are obtained for singlet O_2 using either restricted or unrestricted wavefunctions in the DFT calculation. When the Au–O separation (for the nearest O) is between 4.0

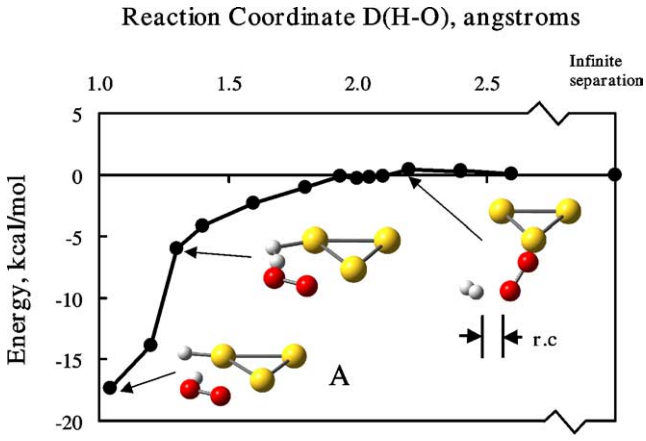

Fig. 3. The unactivated addition of hydrogen to the Au_3O_2 cluster is the final step in the entrance channel of the catalytic cycle to form intermediate **A**. Hydrogen attack of the di-oxygen group generates a hydroperoxy intermediate and after H–H bond scission, a Au–H bond is formed helping to stabilize the hydroperoxy fragment. The final intermediate **A** has a planar geometry.

and 5.0 Å, the energy of the doublet spin system is approximately the same as for the quartet spin system. In this region of approach, the spin transition can occur as an unactivated process. The equilibrium Au–O bond distance in the intermediate **2** is 2.138 Å, and the binding energy for O_2 on triangular Au_3 is 19 kcal/mol. Given that an unactivated attack of O_2 can lead to such a stable oxide, Au_3O_2 (**2**) is likely the preferred geometry for such a Au nanoparticle in air (or with another O_2 adsorbed as well, in similar end-on fashion, as found by Mills et al. [54]).

Oxygen molecule also reacts with Au_3 having a linear geometry. We observed a shallow energy plateau near geometries with O_2 adsorbed in end-on fashion to a slightly bent linear Au_3 cluster. Relaxation of these geometries often proceeded to the triangular Au geometry with end-on bent O_2 (intermediate **2**). A locally stable structure with crooked linear Au_3 geometry and end-on bonded O_2 was identified with an energy 4 kcal/mol higher than for intermediate **2**. The Au–Au–Au angle in the crooked linear configuration was 118.5°.

After forming the stable Au_3O_2 structure **2**, the next step in the entrance channel is reaction with molecular hydrogen, which is also energetically downhill and unactivated as detailed in Fig. 3. As H_2 approaches the oxygen atom farthest from the Au cluster, interaction begins near H–O separation of approximately 2.5 Å. Near a separation of 2.0 Å there may be a shallow stable state of preadsorbed hydrogen, but this geometry was not found. As H_2 continues to react with the cluster both O–O and H–H rotate into the same plane as the Au atoms. The final intermediate state **A** is planar and has H directly bonded to one Au atom and a hydroperoxy-like species (–OOH) anchored to one side of the Au cluster. Direct desorption of the neutral hydroperoxy radical from **A** requires 23.3 kcal/mol and is not likely to be part of a viable mechanism for epoxidation of propylene (by transfer to the active Ti site in TS-1, for example).

3.3. Catalytic cycle

The catalytic cycle proceeds through several steps: (1) activated addition of molecular hydrogen, (2) desorption of the product H_2O_2, followed by (3) the exothermic addition of molecular oxygen to form an intermediate **D**, which rearranges to regenerate hydroperoxy intermediate **A** allowing the cycle to repeat. The cycle is illustrated in Fig. 1. Individual reaction steps are discussed in separate sections below. The completed cycle is calculated to be exothermic by 28.2 kcal/mol consistent with the thermodynamics of the net reaction $H_2 + O_2 \rightarrow H_2O_2$. The activation barriers are 7.2 kcal/mol for H_2 addition to intermediate **A** to form **TS A** and 2.6 kcal/mol for structural rearrangement from **D** to **TS D**. Addition of O_2 to the intermediate **C** is unactivated. The other energy barrier in the cycle is desorption of the product H_2O_2 which requires 8.6 kcal/mol. This would be the inferred rate-limiting step in kinetically limited production of H_2O_2.

The electron population based on Natural Bond Orbital analysis [49] for the three Au atoms in the various clusters in the cycle is shown in Fig. 1. The net charge on Au_3 varies from a high of +0.390 for the entrance channel intermediate **2**, to as low as −0.138 in intermediate **C.** Variation in net charge on the cluster over the complete cycle makes it difficult to characterize the state of gold as being one charge type of the other, but the predominant state in the cycle itself is largely cationic (delta plus charge) as the electronegativity of oxygen is greater than that of gold. The highest energy barrier around the cycle is for desorption of H_2O_2 from intermediate **B** (vide infra) which makes this state with NBO charge of +0.185, partially cationic, the most likely observed during reaction. Under ambient conditions when exposed to oxygen, the Au cluster is likely to have one (**2**, NBO charge +0.390) or two oxygen molecules adsorbed and be in a cationic charge state. While these findings are consistent with the active form of gold being cationic [22,56], the question of whether the reactivity can be altered by enhancing the cationic character of the gold cluster has not yet been addressed computationally. Such calculations are now in progress.

Many of the intermediate geometries are planar, but both the entry channel and the addition of oxygen in the cycle are more energetically favorable for approach in directions normal to the plane of the trimer cluster. Interestingly, only one side of the cluster needs to be unhindered to accommodate these steps in the reaction mechanism. A cluster anchored on a support surface with only one side exposed to the gas phase would still be able to accommodate the proposed reaction mechanism provided the electronic perturbation did not inhibit the reactions. DFT calculations we have made suggest the interactions of the cluster with a support like TS-1 are weak (on the order of 5 kcal/mol). Compared to the electron populations shifts during the catalytic cycle, the interaction of a bare Au trimer with model clusters of a Ti site in TS-1 (having 10 tetrahedral Si plus 1 tetrahedral Ti centers) was

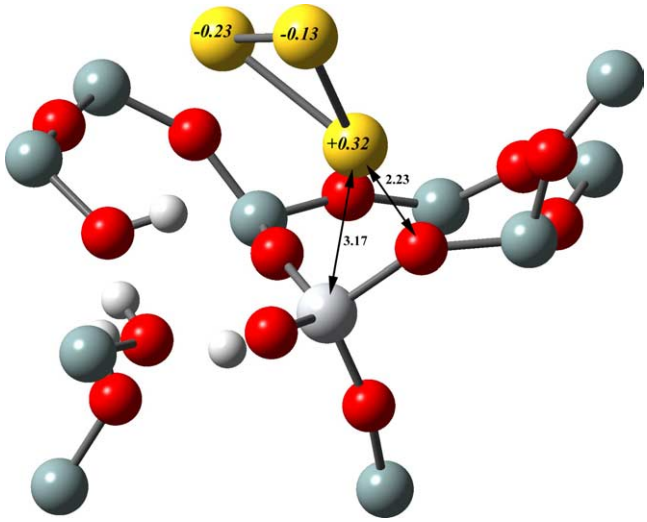

Fig. 4. Neutral Au_3 cluster adsorbed on a cluster model of a proposed active site in TS-1. NBO electron populations are the signed values inside yellow Au atoms. Oxygen ions are red, silicon bluish gray, hydrogens in the silanol nest are small white spheres, and the large white sphere is titanium in the T6 position. Terminating hydrogens to maintain the zeolite structure are not shown. Distances indicated are in angstroms.

essentially neutral with a shift in the net electron population of −0.044 unit (more electron density on the trimer when supported). The binding energy for Au_3 on the model TS-1 cluster as shown in Fig. 4 was only 5.7 kcal/mol coming from a weak interaction between one of the Au atoms and an oxygen ion in the support. The minimum Au–O distance for this interaction was 2.23 Å.

3.4. Addition of hydrogen

Besides the desorption of the product H_2O_2, the breaking of the H–H bond is the most energetically demanding step in this catalytic cycle. H–H bond breakage occurs at two points in the mechanism, going from intermediate **2** to intermediate **A** and from intermediate **A** to transition state **TS A**.

Structure **A** can be taken as the starting point for the catalytic cycle that generates H_2O_2. Gas-phase H_2 attacks this complex to form intermediate **B** via transition state **TS A.** Unlike the H_2 addition in the entrance channel, H_2 addition in the catalytic cycle is activated and proceeds through a stable adsorbed H_2 configuration not shown in Figs. 1 and 5. This configuration is very close in energy to the transition state and was not considered important in mapping out the major features of this cycle. In both the stable preadsorbed state and at the transition state, H_2 inserted between the oxygen end of the hydroperoxy group and the nearest Au atom. The motion at the transition state **TS A** associated with the imaginary frequency is mainly an H–H bond stretch leading directly to the intermediate **B**, where this bond has been broken. Given the location of the two H atoms, this bond breaking is also necessarily directly associated with formation of one O–H and one H–Au bond. The energy barrier to reach the transition state is 7.2 kcal/mol above the energy of intermediate **A** and gas-phase molecular hydrogen (see Fig. 5).

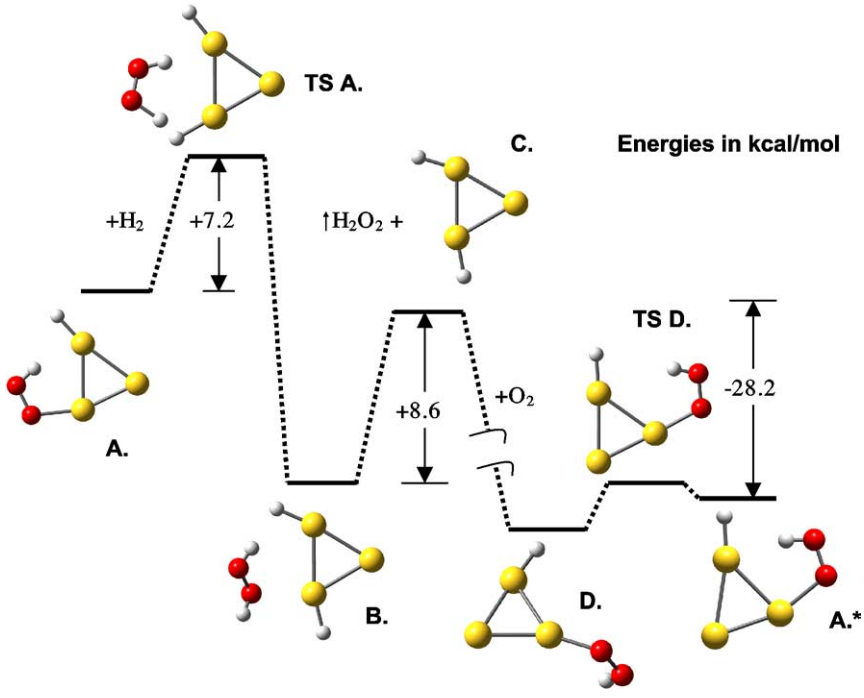

Fig. 5. Energetics and geometries for the catalytic cycle forming hydrogen peroxide over neutral Au trimer from H_2 and O_2. The final configuration **A*** rotated by 180° is equivalent to intermediate **A**. Or, the reaction steps can be followed around the cycle a second time (see text) which may be important for a cluster sitting on a support surface that is only accessible from one side.

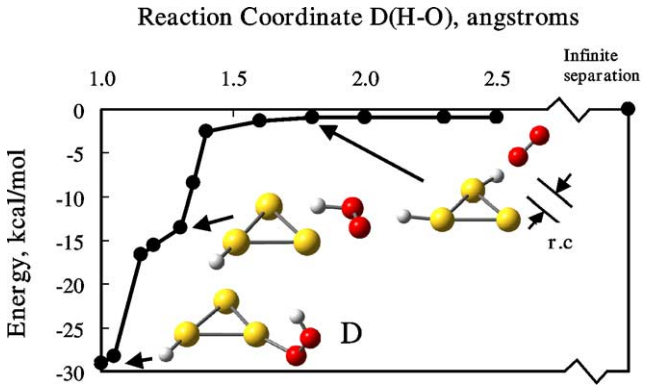

Fig. 6. The energy profile (at 0 K without zero-point energy corrections) for oxygen addition to intermediate **C** to form intermediate **D**. Once formed, the hydroperoxy intermediate rotates out of the Au_3 plane and bonds via the terminal oxygen end to the Au cluster in intermediate **D**.

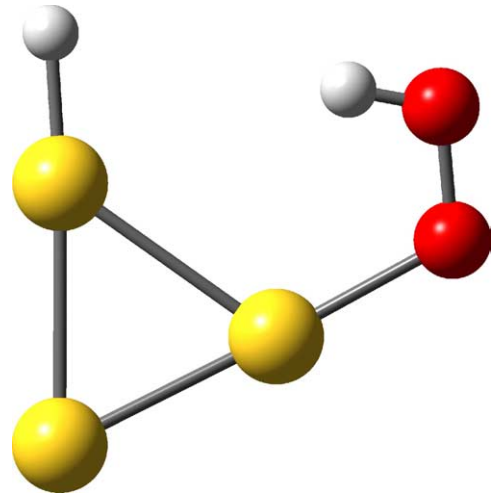

Fig. 7. Transition State D (**TS D**) where the hydroperoxy group is almost rotated back down into the Au_3 plane to form intermediate **A**.

3.5. *Desorption of hydrogen peroxide*

Hydrogen peroxide adsorbed on the Au cluster in intermediate **B** requires 8.6 kcal/mol to desorb and leaves behind intermediate **C**. This is the largest energy barrier in the catalytic cycle. The desorption proceeds with relatively low or no activation energy as there are no strong bonds between the hydrogen peroxide molecule and the remaining Au_3H_2 cluster to break. The peroxide molecule is adsorbed on the edge of the Au_3 cluster and is canted slightly above and below the Au_3 plane. Though the energy of desorption is the highest energy step in the formation of hydrogen peroxide, it is smaller than the most energetic step in the subsequent epoxidation reaction by hydrogen peroxide over TS-1. Our previous DFT calculations on epoxidation of propylene by H_2O_2 gave a maximum barrier height at 15.4 kcal/mol [35]. This implies that the rate-limiting step for the overall reaction of $H_2 + O_2 +$ propylene to propylene oxide $+ H_2O$ over Au/TS-1 is not in the formation of H_2O_2, but in the epoxidation steps. Specifically, it occurs when H_2O_2 reacts with an open Ti site of TS-1 to form a reactive hydroperoxy intermediate.

3.6. *Addition of oxygen*

Addition of di-oxygen to the intermediate **C** is detailed in Fig. 6. This reaction step is the most exothermic (−29.1 kcal/mol) and is the largest single energetic transition of the mechanism. As O_2 approaches the Au_3H_2 cluster, it pulls off one of the H atoms attached to the cluster. The nearest distance between an O atom of the attacking O–O and the H atom attacked was constrained as the reaction coordinate to determine the energies shown in Fig. 6. At a H–O separation of 1.3 Å, a hydroperoxy fragment formed from the approaching oxygen molecule is bonded to the side of the Au cluster. This fragment is similar to the hydroperoxy species in intermediate **A** but is not stabilized by an adjacent Au–H as is intermediate **A**. Further reaction allows one of the oxygen atoms to begin bonding to an Au atom of the cluster while the H atom of the hydroperoxy breaks its bond to Au at the other end of the cluster. As the reaction coordinate continues past 1.3 Å, the OOH fragment now bonded by the terminal O atom to the cluster rotates up out of the plane of the Au cluster. The net effect has been to insert O–O into a Au–H bond with no activation energy. However, the OOH is bonded via oxygen to a different Au atom of the cluster than the original Au–H.

3.7. *Closure of the catalytic cycle*

The final mechanistic step in closing the catalytic cycle is the rotation of the hydroperoxy group which is oriented perpendicular to the Au_3 plane in intermediate **D** down into the Au_3 plane to form a geometry equivalent to the starting geometry **A**. This rotation proceeds through transition state **TS D** which requires crossing a small +2.6 kcal/mol energy barrier. Fig. 7 has details of the transition state geometry. Comparison of transition state **TS D** with intermediate **A** (see Fig. 1) shows that the hydroperoxy group has ended up on a different side of the Au cluster. The true original geometry of intermediate **A** is obtained by rotating the structure 180° about an axis lying in the Au_3 plane (the axis of the H–Au bond as indicated in Fig. 1, **TS D**). Formally this completes the cycle, but as we envision this cycle occurring on a Au_3 cluster supported in or on a TS-1 crystallite, there are a few details to consider. In the particular case of a supported cluster, only free space on one side of the Au cluster should be available since (a) the support may block the other side, and (b) rotation of the cluster may not be possible. Even with these two limitations, the cycle of Fig. 1 can proceed.

There are two structures with three-dimensional geometries—intermediates **B** and **D** (and closely related **TS D**, but if the intermediate **D** can be accommodated, so can the transition state). Intermediate **B** is only slightly three dimensional due to hydrogen peroxide bonded to one edge of the Au_3 cluster. One of the oxygen atoms is slightly above the

Table 1
Thermochemical data for stable configurations, molecules, and transition states[a]

Configuration or molecule[h]	E[b] (0 K) (Hartree)[g]	ZPE[c] (Hartree)[g]	U[d] (298 K) (Hartree)[g]	G[e] (298 K) (Hartree)[g]	ln(Q)[f]
1	−406.59371	0.00068	−406.58798	−406.62955	37.95583
2	−556.94161	0.00495	−556.92830	−556.97817	38.71874
A	−558.14107	0.02149	−558.11039	−558.16105	21.16261
TS A	−559.30129	0.03222	−559.25920	−559.31142	10.73019
B	−559.32775	0.03905	−559.27784	−559.33166	4.13386
C	−407.77982	0.01302	−407.76034	−407.80362	25.20920
D	−558.14377	0.02220	−558.11222	−558.16290	20.26179
TS D	−558.14066	0.02206	−558.10910	−558.16089	21.42583
O_2	−150.31755	0.00310	−150.31208	−150.33454	17.99215
H_2	−1.17174	0.00996	−1.15942	−1.17328	1.63212
H_2O_2	−151.53418	0.02422	−151.50645	−151.53207	−2.23449

[a] Vibration along the reaction coordinate (imaginary frequency) is ignored in the thermal corrections at 298 K.
[b] Without zero-point energy (ZPE) corrections added. Note the predicted energy fluctuation at convergence of these geometries was $\lesssim 1.0 \times 10^{-6}$ Hartree.
[c] Zero-point energy.
[d] U, internal energy with all thermal corrections to 298 K added.
[e] G, Gibb's free energy with all thermal corrections to 298 K added.
[f] Q is the partition function.
[g] 1 Hartree = 627.5095 kcal/mol.
[h] See Fig. 1 for schematic geometries of these configurations.

Au_3 plane and the other slightly below. Since the geometry is only slightly out of plane, it should not interfere with a support material. Intermediate **D** is three dimensional due to the hydroperoxy group extending up out of the Au_3 plane. This hydroperoxy group can be formed on either side of the planar starting intermediate **C**, so this reaction step can avoid steric hindrance from a support surface as well. It remains to show that the cycle will close without requiring a 180° rotation (see Fig. 1, **TS D**).

Supposing an anchored cluster would not be free to rotate, the intermediate **A** can be regenerated from **TS D** by simply making another transit of the cycle using the opposite edge of the cluster. Geometries **A′**, **TS A′**, **B′**, **C′**, **D′**, and **TS D′** of the second transit illustrating the chemistry on the opposite side of the Au_3 cluster are shown in Fig. 8. Each primed structure is actually identical to the corresponding unprimed structure in Fig. 1 (rotated by 180° about the axis of the H–Au bond) but is shown here to make the second transit easier to follow. In forming intermediate **D′** we utilize the flexibility of this intermediate to form on either side (face) of the Au_3 cluster (vide supra). This shows that the catalytic cycle can occur on the same side of the Au cluster without requiring access to the other side and is thus quite applicable not only to a gas-phase process, but to the case of a supported cluster as well.

3.8. Thermochemistry

Table 1 shows the calculated thermochemical data for each intermediate and transition state identified above. These values are the results from Gaussian frequency calculations at the same level of DFT theory used to identify the geometries. Internal energy (U) and Gibb's free energy (G) values were calculated for 298.15 K and 1 atm pressure. The thermodynamics of each reaction step at 298.15 K and 1 atm are shown in Table 2. Under these conditions the H_2O_2 desorption barrier actually has a negative Gibb's free energy change, −2.5 kcal/mol, due to the favorable entropic change. The energetic barrier at 0 K for this step is +8.6 kcal/mol without zero-point energy corrections. The reaction step with the largest Gibb's free energy change, +14.4 kcal/mol, is forming the transition state **TS A** after attack of H_2 on intermediate **A** which requires dissociation of H_2 along the reaction coordinate. The net Gibb's free energy change for the entire catalytic cycle is −15.2 kcal/mol at 298.15 K and 1 atm pressure. Under these conditions, the net Gibb's free energy change of the overall entrance channel reaction, $Au_3 + H_2 + O_2$, is −14.9 kcal/mol and as discussed above is an unactivated process.

Table 2
Thermochemical data for reactions

Reaction	ΔU[a] (0 K) (kcal/mol)	ΔU[b] (298 K) (kcal/mol)	ΔG[b] (298 K) (kcal/mol)
1 + O_2 → **2**	−19.0	−17.7	−8.8
2 + H_2 → **A**	−17.4	−14.2	−6.0
A + H_2 → **TS A**	7.2	6.7	14.4
TS A → **B**	−16.6	−11.7	−12.7
B → **C** + H_2O_2	8.6	6.9	−2.5
C + O_2 → **D**	−29.1	−25.0	−15.5
D → **TS D**	2.0	2.0	1.3
TS D → **A**	−0.3	−0.8	−0.1

[a] Without ZPE correction.
[b] With all thermal corrections to 298 K added.

4. Conclusions

A complete mechanism for the epoxidation of propylene by H_2 and O_2 over Au/TS-1 catalysts based on DFT calculations can now be put forward for the first time. We

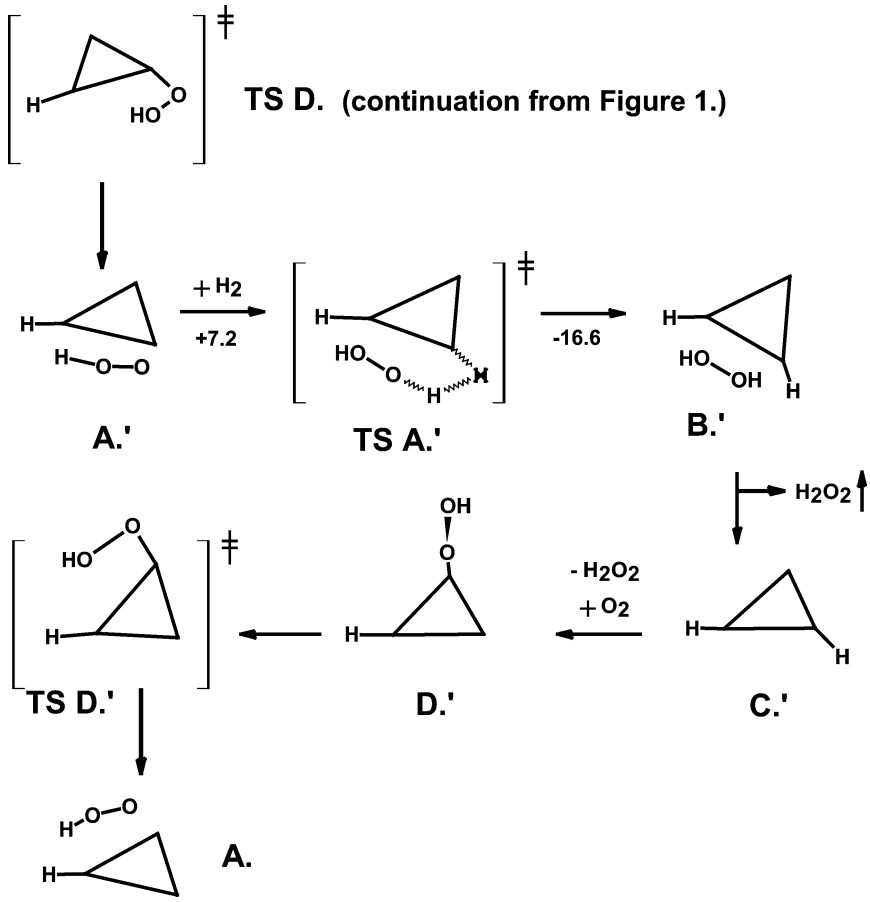

Fig. 8. A second transit of the catalytic cycle shown in Fig. 1 to demonstrate regeneration of the starting intermediate **A**. Each intermediate and transition state labeled with a prime is geometrically equivalent (after a "pancake flip" of the Au_3 cluster) to the corresponding unprimed structure of Fig. 1. This also demonstrates that the catalytic cycle can operate using only access to one side of the Au_3 cluster.

believe the mechanism presented above for formation of hydrogen peroxide from H_2 and O_2 over a Au_3 cluster gives a plausible account of the role of Au in this catalyst. We acknowledge that there may be other reaction paths to propylene oxide. Certainly this explanation is at odds with existing notions that relatively larger Au nanoparticles (∼2 nm) are most active for epoxidation. However, experimental work in our laboratory has shown that besides the visible Au seen in TEM images of the Au/TS-1 system, there is a great deal, possibly 80% of the Au present, which is smaller than 1 nm [57]. A bare Au_3 cluster has a diameter of approximately 0.3 nm. Even with additional reacting adducts, it would fit inside the 0.5-nm TS-1 pore system in proximity to active Ti epoxidation sites. The Au_3 cluster could also anchor on the external surface of the support. A small Au cluster with access to H_2 and O_2 could provide a supply of in situ-generated H_2O_2 for reaction with propylene. Coupled with our recently published mechanism, based on DFT calculations, for propylene epoxidation via a hydroperoxy intermediate on Ti sites adjacent to Si vacancies [35], these two mechanisms give a viable account of the formation of propylene oxide from propylene in this system. Even if this picture is not the explanation for current Au/TS-1 catalysts, there is good reason to consider new materials based on this mechanism, and work continues in our lab on these ideas.

Acknowledgments

D.H.W. thanks Shell Oil Company for fellowship funding. This work was also funded through the National Science Foundation Grant CTS-0238989-CAREER (K.T.T.). The authors acknowledge Purdue University Computing Center's Research Computing Division and the NCSA computing facility at the University of Illinois where the majority of the calculations were made. Computations at the University of Illinois were made possible by a grant from the Department of Energy. We also acknowledge support by the Chemical Sciences, Geosciences, and Biosciences Division, Office of Basic Energy Sciences, Office of Science, US Department of Energy Grant DE-FG02-01ER15107.

References

[1] G. Li, X. Wang, H. Yan, Y. Liu, X. Liu, Appl. Catal. A 236 (2002) 1–2.
[2] S. Bordiga, A. Damin, F. Bonino, A. Zecchina, G. Spanò, F. Rivetti, V. Bolis, C. Prestipino, C. Lamberti, J. Phys. Chem. B 106 (2002) 9892.

[3] T.A. Nijhuis, B.J. Huizinga, M. Makkee, J.A. Moulijn, Ind. Eng. Chem. Res. 38 (1999) 884.
[4] A. Bhaumik, T. Tatsumi, J. Catal. 182 (1999) 349.
[5] Y. Hasegawa, A. Ayame, Catal. Today 71 (2001) 177.
[6] P.F. Henry, M.T. Weller, C.C. Wilson, J. Phys. Chem. B 105 (2001) 7452.
[7] E. Duprey, P. Beaunier, M.-A. Springuel-Huet, F. Bozon-Verduraz, J. Fraissard, J.-M. Manoli, J.-M. Brégeault, J. Catal. 165 (1997) 22.
[8] E. Karlsen, K. Schöffel, Catal. Today 32 (1996) 107.
[9] C. Qi, T. Akita, M. Okumura, M. Haruta, Appl. Catal. A 218 (2001) 81.
[10] G. Ricchiardi, A. Damin, S. Bordiga, C. Lamberti, G. Spanö, F. Rivetti, A. Zecchina, J. Am. Chem. Soc. 123 (2001) 11409.
[11] C.B. Khouw, C.B. Dartt, J.A. Labinger, M.E. Davis, J. Catal. 149 (1) (1994) 195.
[12] R. Meiers, U. Dingerdissen, W.F. Holderich, J. Catal. 176 (2) (1998) 376.
[13] X.-W. Guo, X.-S. Wang, M. Lui, G. Li, Y. Chen, J. Xiu, J. Zhuang, W. Zhang, X.-H. Bao, Catal. Lett. 81 (1–2) (2002) 125.
[14] K. Chaudhari, D. Srinivas, P. Ratnasamy, J. Catal. 203 (1) (2001) 25.
[15] A. Bhaumik, T. Tatsumi, J. Catal. 176 (2) (1998) 305.
[16] W. Laufer, R. Meiers, W. Holderich, J. Mol. Catal. A: Chem. 141 (1–3) (1999) 215.
[17] A.J.H.P. van der Pol, A.J. Verduyn, J.H.C. van Hooff, Appl. Catal. A 92 (2) (1992) 113.
[18] A. Tuel, Y.B. Taarit, Appl. Catal. A 110 (1) (1994) 137.
[19] R.S. Drago, S.C. Dias, J.M. McGilvray, A.L.M.L. Mateus, J. Phys. Chem. B 102 (1998) 1508.
[20] M. Taramasso, G. Perego, B. Notari, Patent 4,410,501 (1983).
[21] T. Hayashi, K. Tanaka, M. Haruta, J. Catal. 178 (2) (1998) 566.
[22] Q. Fu, H. Saltsberg, M. Flyzani-Stephanopoulos, Science 301 (2003) 935.
[23] J. Guzman, B.C. Gates, J. Phys. Chem. B 106 (2002) 7659.
[24] J. Guzman, B.C. Gates, J. Am. Chem. Soc. 126 (2004) 2672.
[25] M. Mavrikakis, P. Stoltze, J.K. Nørskov, Catal. Lett. 64 (2–4) (2000) 101.
[26] D.M. Cox, R. Brickman, K. Creegan, A. Kaldor, Z. Phys. D 19 (1991) 353.
[27] P. Landon, P.J. Collier, A.J. Papworth, C.J. Kiely, G.J. Hutchings, Chem. Commun. 2002 (2002) 2058.
[28] C. Sivadinarayana, T.V. Choudhary, L.L. Daemen, J. Eckert, D.W. Goodman, J. Am. Chem. Soc. (2003).
[29] M.G. Clerici, G. Bellussi, U. Romano, J. Catal. 129 (1991) 159.
[30] G. Bellussi, A. Carati, M.G. Clerici, G. Maddinelli, R. Millini, J. Catal. 133 (1992) 220.
[31] M.G. Clerici, P. Ingallina, J. Catal. 140 (1993) 71.
[32] P.E. Sinclair, C.R.A. Catlow, J. Phys. Chem. B 103 (1999) 1084.
[33] P.E. Sinclair, G. Sankar, C.R.A. Catlow, J.M. Thomas, T. Maschmeyer, J. Phys. Chem. B 101 (1997) 4232.
[34] H. Munakata, Y. Oumi, A. Miyamoto, J. Phys. Chem. B 105 (2001) 3493.
[35] D.H. Wells Jr., H. David, W.N. Delgass, K.T. Thomson, J. Am. Chem. Soc. 126 (2004) 2956.
[36] C. Lamberti, S. Bordiga, A. Zecchina, G. Artioli, G.L. Marra, G. Spanò, J. Am. Chem. Soc. 123 (2001) 2204.
[37] M.J. Frisch, G.W. Trucks, H.B. Schlegel, G.E. Scuseria, M.A. Robb, J.R. Cheeseman, V.G. Zakrzewski Jr., R.E. Stratmann, J.C. Burant, S. Dapprich, J.M. Millam, A.D. Daniels, K.N. Kudin, M.C. Strain, O. Farkas, J. Tomasi, V. Barone, M. Cossi, R. Cammi, B. Mennucci, C. Pomelli, C. Adamo, S. Clifford, J. Ochterski, G.A. Petersson, P.Y. Ayala, Q. Cui, K. Morokuma, D.K. Malick, A.D. Rabuck, K. Raghavachari, J.B. Foresman, J. Cioslowski, J.V. Ortiz, A.G. Baboul, B.B. Stefanov, G. Liu, A. Liashenko, P. Piskorz, I. Komaromi, R. Gomperts, R.L. Martin, D.J. Fox, T. Keith, M.A. Al-Laham, C.Y. Peng, A. Nanayakkara, M. Challacombe, P.M.W. Gill, B. Johnson, W. Chen, M.W. Wong, J.L. Andres, C. Gonzalez, M. Head-Gordon, E.S. Replogle, J.A. Pople, Gaussian98, 1998.
[38] A.D. Becke, Phys. Rev. A 38 (1988) 3098.
[39] K. Burke, J.P. Perdew, Y. Wang, in: J.F. Dobson, G. Vignale, M.P. Das (Eds.), Electronic Density Functional Theory: Recent Progress and New Directions, Plenum, New York, 1998.
[40] J.P. Perdew, K. Burke, Y. Wang, Phys. Rev. B 54 (23) (1996) 16533.
[41] J.P. Perdew, J.A. Chevary, S.H. Vosko, K.A. Jackson, M.R. Pederson, D.J. Singh, C. Fiolhais, Phys. Rev. B 46 (1992).
[42] J.P. Perdew, J.A. Chevary, S.H. Vosko, K.A. Jackson, M.R. Pederson, D.J. Singh, C. Fiolhais, Phys. Rev. B 48 (1993).
[43] P.J. Hay, W.R. Wadt, J. Chem. Phys. 82 (1985) 270.
[44] P.J. Hay, W.R. Wadt, J. Chem. Phys. 82 (1985) 299.
[45] J.T.H. Dunning, P.J. Hay, in: I.H.F. Schaefer (Ed.), Modern Theoretical Chemistry, Plenum, New York, 1976, vol. 3.
[46] P.C. Redfern, J.-P. Blaudeau, L.A. Curtiss, J. Phys. Chem. A 101 (1997) 8701.
[47] D.H. Wells, W.N. Delgass, K.T. Thomson, J. Chem. Phys. 117 (23) (2002) 10597.
[48] C. Peng, H.B. Schlegel, Israel J. Chem. 33 (1993) 449.
[49] E.D. Glendening, A.E. Reed, J.E. Carpenter, F. Weinhold, NBO Version 3.1.
[50] G. Bravo-Pérez, I.L. Garzón, O. Novaro, J. Mol. Struct. (Theochem) 493 (1999) 225.
[51] H. Grönbeck, W. Andreoni, Chem. Phys. 262 (2000) 1.
[52] B. Yoon, H. Häkkinen, U. Landman, J. Phys. Chem. A 107 (2003) 4066.
[53] M. Okumura, Y. Kitagawa, M. Haruta, K. Yamaguchi, Chem. Phys. Lett. 346 (2001) 163.
[54] G. Mills, M.S. Gordon, H. Metiu, Chem. Phys. Lett. 359 (2002) 493.
[55] M. Ardon, Oxygen—Elementary Forms and Hydrogen Peroxide, Benjamin, New York, 1965.
[56] A. Kuperman, US Patent 6,255,499 (2001).
[57] N. Yap, R.P. Andres, W.N. Delgass, submitted.